Journal of Colloid and Interface Science 638 (2023) 719–732

Contents lists available at ScienceDirect

Journal of Colloid and Interface Science

journal homepage: www.elsevier.com/locate/jcis

Phase separation in a ternary DPPC/DOPC/POPC system with reducing hydration

Christopher J. Garvey [a,*], Saffron J. Bryant [b], Aaron Elbourne [b], Taavi Hunt [b], Ben Kent [c,d], Martin Kreuzer [d,e], Markus Strobl [d,f], Roland Steitz [d], Gary Bryant [b,*]

[a] Heinz Maier-Leibnitz Zentrum (MLZ), Technische Universität München, Lichtenbergstraße 1, 85748 Garching, Germany
[b] School of Science, RMIT University, Melbourne, Australia
[c] Centre for Advanced Macromolecular Design, School of Chemistry, The University of New South Wales, Sydney 2052, Australia
[d] Institute for Soft Matter and Functional Materials, Helmholtz Zentrum Berlin, Hahn-Meitner-Platz 1, Berlin, Germany
[e] ALBA Synchrotron, Barcelona, Spain
[f] Laboratory for Neutron Scattering and Imaging, Paul Scherrer Institut, 5232 Villigen, Switzerland

GRAPHICAL ABSTRACT

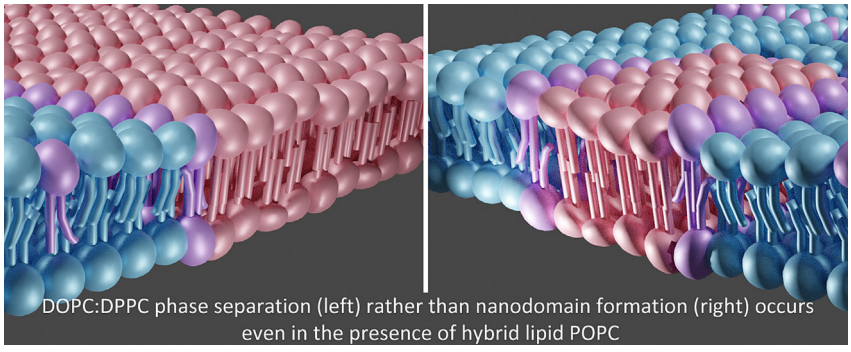

ARTICLE INFO

Article history:
Received 26 October 2022
Revised 10 January 2023
Accepted 31 January 2023
Available online 3 February 2023

Keywords:
Membranes
Phospholipids
Domains
Lineactants
Neutron scattering
X-ray Scattering
AFM
Phase separation

ABSTRACT

The maintenance of plasma membrane structure is vital for the viability of cells. Disruption of this structure can lead to cell death. One important example is the macroscopic phase separation observed during dehydration associated with desiccation and freezing, often leading to loss of permeability and cell death. It has previously been shown that the hybrid lipid 1-palmitoyl-2-oleoyl-*sn*-*glycero*-3-phosphocholine (POPC) can act as a line-active component in ternary lipid systems, inhibiting macroscopic phase separation and stabilising membrane microdomains in lipid vesicles [1]. The domain size is found to decrease with increasing POPC concentration until complete mixing is observed. However, no such studies have been carried out at reduced hydration. To examine if this phase separation is unique to vesicles in excess water, we have conducted studies on several binary and ternary model membrane systems at both reduced hydration ("powder" type samples and oriented membrane stacks) and in excess water (supported lipid bilayers) at 0.2 mol fraction POPC, in the range where microdomain stabilisation is reported. Differential scanning calorimetry (DSC) and Fourier transform infrared spectroscopy (FTIR) are used to map phase transition temperatures, with X-ray and neutron scattering providing details of the changes in lipid packing and phase information within these boundaries. Atomic force microscopy (AFM) is used to image bilayers on a substrate in excess water. In all cases, macroscopic phase separation was observed rather than microdomain formation at this molar ratio. Thus POPC does not stabilise microdomains under these conditions, regardless of the type of model membrane, hydration or temperature. Thus we conclude

* Corresponding authors.
E-mail addresses: christopher.garvey@tum.de (C.J. Garvey), gary.bryant@rmit.edu.au (G. Bryant).

https://doi.org/10.1016/j.jcis.2023.01.145

that the driving force for separation under these conditions overcomes any linactant effects of the hybrid lipid.

1. Introduction

Cell membranes—bilayers formed by lipid molecules—have functions far beyond that of passive barriers for free diffusion. The maintenance of transport properties of the plasma membrane is an important aspect of the viability of cells in dry or freezing conditions [2] and research continues to reveal the role of the cell membrane lipids in vital processes including signalling, nutritional uptake, lipid turnover in the membrane, and coupling with the cytoskeleton.[3] In 1972 Singer and Nicolson proposed the Fluid Mosaic Model of cell membranes which posited a random two-dimensional distribution of lipids and proteins in the bilayer.[4] Although very successful in understanding many aspects of biological membranes this conceptual framework is limited, and omits spatial complexities such as the idea of 'lipid rafts', which represent regions of a membrane where there is some lateral degree of segregation of lipids and other membrane components to create organized microdomains within the bilayer.[5] This concept is an important improvement to the model which can explain many functionalities of the plasma membrane. Rafts are domains in cell membranes which contain molecular compositions distinct from their surroundings in the 2-dimensional milieu of the lipid bilayer. The formation of rafts facilitates lateral organisation of membrane components with important consequences in, for example, membrane signalling and trafficking[6,7]. The size of these heterogeneities are thought to be in the range of 10–100 nm.[8].

Despite their importance, our understanding of the physicochemical principles under-pinning the formation and stability of lipid rafts is lacking. The work of Safran and subsequent computational works have suggested a simple mechanistic control of domain number and size based on the lipid membrane composition.[9] While cell membranes are quite complex, containing hundreds of different lipid species, with asymmetric leaflets as well as proteins and other molecules,[10] symmetric model membranes, containing three or fewer lipid species, can reveal simple principles around the stabilisation of the phase separation of mixtures for lipids with saturated and unsaturated hydrocarbon tail groups. [11] In this case the theoretical investigations indicate that phase separation should be driven by specific mechanisms including the line-tension between regions of saturation and unsaturation; and the energetic cost of hydrophobic mis-match due to slight differences in the thickness of bilayers. These effects will drive thermodynamic phase separation. Theoretical investigations [12–14] have explored the potential for thermodynamic stability of small domains in ternary systems where the thermodynamic cost of the interface between the phases of saturated and unsaturated lipid is minimised by line-active agents, known as ''linactants''. This theoretical work has focussed on ternary mixtures containing lipids with the phosphatidylcholine headgroup, with the two majority lipids containing equivalent lengths of saturated and unsaturated chains. The driving force for phase separation is diminished by the addition of the linactant, which contains one saturated and one unsaturated chain. Research has shown that different molecules may reduce line tension and allow nanodomain formation, including cholesterol,[15,16] short lipids,[17–19] and impurities.[20] More broadly, it is generally agreed that lipid rafts in the plasma membrane can form into either macrodomains (type 2) or nanodomains (type 1) depending on the presence of linactants and the types of lipids involved.[3,21] These ordered domains are usually rich in saturated lipids as well as cholesterol (if it is present in the system), and are surrounded by the disordered, continuous domain which is rich in unsaturated lipids.[15].

Most experimental work to date has been in excess water and with lipids in the fluid phase at room temperature. However, there are many applications where lipid phase separations and domain formation have been implicated in damage at either reduced hydration, such as desiccation[22] and freezing damage,[23,24] or at temperature extremes, such as in chilling damage[25] and modulation of heat stress[26] in plants.

In this study we experimentally examine the hydration and temperature dependent effects of the linactant 1-palmitoyl-2-oleoyl-*sn-glycero*-3-phosphocholine (POPC) on the phase behaviour of mixtures containing 1,2-dipalmitoyl-phosphatidylcholine (DPPC) and 1,2-dioleoyl-phosphatidylcholine (DOPC). POPC contains one palmitoyl (saturated) and one oleoyl (unsaturated) tail, which are common to DPPC and DOPC respectively (Fig. 1). In previous work on such a system, Szekely *et al.* explored mixtures of DPPC and DOPC with different mole ratios of the hybrid lipid POPC.[1] They took advantage of the affinity of calcium ions to DPPC as a probe and found that the addition of POPC allowed formation of stable nanodomains, the size of which decreased with increasing amounts of POPC. For a DOPC:DPPC molar ratio of 1:1, molar ratios of POPC beyond 0.3 resulted in complete mixing of all three lipids and the disappearance of the nanodomains.[1] More recently, Hitaishi *et al.*[27]showed that in ternary systems POPC mixes well with DOPC and leads to an increase in bilayer thickness, but only has a small effect on DPPC, and the authors speculate that the POPC may concentrate on the boundaries of the DOPC domains if domains are present.

In this paper we examine for the first time the effect of different levels of hydration on such systems, focussing on POPC ratios where nanodomains have been previously observed.[1] We use X-ray and neutron scattering to explore if the hybrid lipid has similar effects at reduced hydration (where driving forces for phase separation are potentially stronger [2,28]). We also use Atomic Force Microscopy (AFM) to see if the effects are evident in the topography of supported lipid bilayers in excess water.

2. Materials and methods

2.1. Lipid preparation for Scattering, Spectroscopic, and Synchrotron studies

Synthetic phospholipids (<99 % purity) were obtained from Avanti Polar-Lipids (Alabaster, USA) and used without further purification. The three lipids were: saturated (1,2-dipalmitoyl-ph osphatidylcholine (DPPC), 16 carbons per chain); unsaturated (1,2-dioleoyl-phosphatidylcholine (DOPC), 18 carbons and one double bond per chain); and a hybrid with chain one of each type (1-palmitoyl-2-oleoyl-phosphatidylcholine, (POPC)). For neutron scattering experiments, DPPC with natural isotopic abundance was exchanged for a tail deuterated analogue with two C16 saturated tails. It is assumed that the tail deuterated analogues of the lipids have very similar phase behaviour to the natural abundance lipids.[29].

Dried lipids were mixed to the desired molar ratios, hydrated with excess deionised water and then sonicated and vortexed to ensure proper mixing. Between vortex mixing, they were exposed

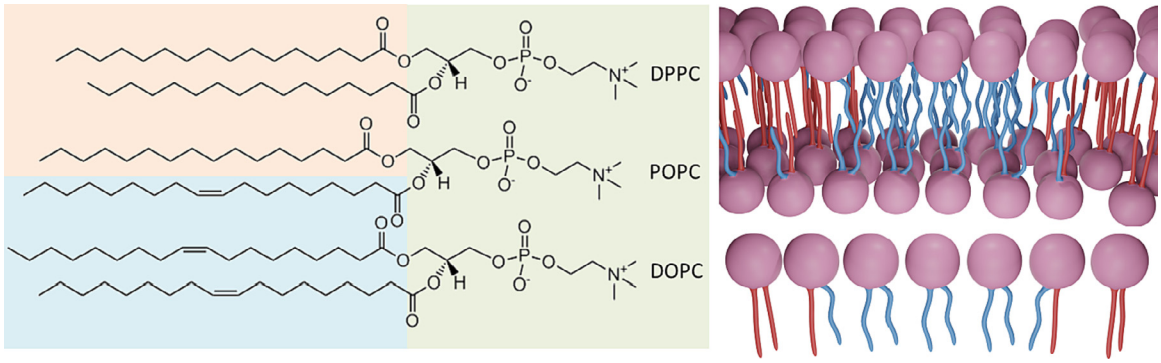

Fig. 1. Left: structures of the lipids used in this study: 1,2-dipalmitoyl-phosphatidylcholine (DPPC), 1-palmitoyl-2-oleoyl-phosphatidylcholine (POPC), and 1,2-dioleoyl-phosphatidylcholine (DOPC). Shaded boxes indicate chemically similar components where the saturated tail of POPC interacts with the saturated tails of DPPC, while the unsaturated tail of POPC interacts with the unsaturated tail of DOPC. Right: Schematic of lipids and resulting macrodomains. Saturated tails are shown in red while unsaturated tails are shown in blue. (For interpretation of the references to colour in this figure legend, the reader is referred to the web version of this article.)

to hot–cold cycles (hot water & liquid nitrogen), to force the lipids through their phase transitions and ensure good mixing. Sample homogeneity was determined by eye. Sample equilibration was confirmed when results (DSC, SAXS) were reproducible after at least two temperature cycles through the gel-fluid transition temperature.

2.2. Controlling relative humidity

For these measurements relative humidity (RH) is the primary control parameter. RH is related to the osmotic pressure Π by:[30]

$$\Pi = -\frac{RT}{V_w} ln\left(\frac{RH}{100}\right)$$

where R is the gas constant, T is the temperature in K and V_w is the partial molar volume of water. Thus by controlling RH, we can ensure that samples have the same osmotic pressure.

In order to control RH, we equilibrate our samples with the vapor phase above saturated salt solutions. Saturated salt solutions are regarded as the most useful method for humidity control, as the RH of the vapor phase above a saturated salt solution has a fixed value at constant temperature.[31]. These values are tabulated in standard references and are accurate to ~ 1 %.

The samples are loaded into pre-weighed pans and incubated at 23 °C above saturated salt solutions that generate known RH [31] as shown in Table S1. Samples are weighed over time, and reach equilibrium once the mass stops changing, which takes a few days for these samples. This will result in slight differences in water content as each lipid hydrates slightly differently. As an example the osmotic pressure and water content are shown for the DOPC:POPC:DPPC system at different RH values in Table S1.

For these experiments samples were equilibrated for 1 week, then transferred to appropriate cells for differential scanning calorimetry (DSC) and small angle X-ray scattering (SAXS) analysis.

2.3. Lipid preparation for AFM studies

Lipid solutions were prepared for AFM using a slightly different protocol. DOPC, POPC, and DPPC lipids were re-hydrated into ultrapure Milli-Q water to a concentration of 1 mg/mL. The solutions were then bath-sonicated at 55 °C for 30 min, subjected to a freeze–thaw cycle (chilled to − 20 °C for 30 min and then bath-sonicated again). At this stage, solutions appeared uniformly "milky", which is known to indicate the formation of multi-lamellar vesicles.[32] The solution was then extruded at least 21 (but always an odd number) of times using a Mini-Extruder kit (Avanti Polar Lipids Inc., AL, USA) with 200 nm filter membranes (Avanti Polar Lipids Inc., AL, USA). This process forms small, unilamellar vesicles (SUVs). The solution was then diluted with 150 mM NaCl to a concentration of 0.01 and 0.1 mg/mL, dependant on the experiment. All glassware, and components had been cleaned thoroughly by sonication with ultrapure water, then isopropyl alcohol, then water again for ten minutes each prior to use. Samples are left to equilibrate for 30 min prior to experiments starting. As lipid mobility is of the order micrometres per second in a bilayer, this is more than sufficient for equilibrium to be achieved.

2.4. DSC experiments

DSC was performed using a Perkin Elmer Pyris DSC with intercooler (Perkin Elmer, Waltham, Massachusetts, USA), calibrated using indium and zinc (Tm(In) 156.6 °C, Tm(Zn) 419.1 °C, ΔH(In) 28.7 J/g, ΔH(Zn) 107.5 J/g). Samples were weighed using a Mettler-Toledo microbalance (accuracy ± 1 μg, Columbus, Ohio, USA) into aluminium pans that were hermetically sealed. Samples were scanned at a rate of 10 °C/min from room temperature to 70 °C (above the gel-fluid transition temperature) and held for four minutes, then cooled at 10 °C/min to −40 °C and held for 2 min before repeating. The entire protocol was repeated at least once to ensure reproducibility. Data was evaluated using Perkin Elmer software, Pyris, and TA Universal Analysis 2000 Version 4.3A. Errors in peak fitting were < ± 1 °C, with differences between runs of ~ ± 1 °C, so errors are set conservatively at ± 2 °C.

2.5. Transmission SAXS experiments

Laboratory SAXS measurements were carried out on two Bruker Nanostar SAXS instruments, both with pinhole geometry. The first instrument, located at RMIT University (Melbourne Australia), has a sealed X-ray tube with a copper anode (Kα radiation, λ = 1.541 Å, operating at 40 kV and 35 mA, sample-to-detector distance 23 cm). The scattering vector, defined as $q = 4\pi\sin(\theta/2)/\lambda$, where θ is the scattering angle and λ is the wavelength of the scattered radiation, covered a range of 0.01–0.4 $Å^{-1}$. The second instrument, located at ANSTO (Lucas Heights, Australia) has a rotating copper anode (Kα radiation, λ = 1.541 Å) where a 72 cm sample to detector distance gives a q range of 0.005–0.35 $Å^{-1}$. Measurements were taken at 10 °C increments between −10 and 60 °C. Temperature control was integrated into data acquisition using the instrument control software. In both cases the raw isotropic 2-dimensional detector images were reduced to the 1d form, I(q), using Bruker software and the instrument geometry. In both cases the measurement time was of the order 10 min.

The SAXS/WAXS beamline at the Australian Synchrotron[33] was used to measure X-ray scattering patterns during cooling. The beamline was configured with a 1.032 Å wavelength and a sample-to-detector distance of 750 mm, giving a q range of 0.09–1.8 $Å^{-1}$. Temperature was controlled with a Linkam Scientific Instrument DSC600 (Guildford, Surrey, England) mounted vertically in the beam. Samples were prepared in hermetically sealed DSC pans and held in place in the vertical configuration using a small spring. The temperature range for each sample was adjusted to encompass the relevant transition temperatures in order to maximise the use of the available beamtime. Samples were warmed at 10 °C/min from room temperature to above the gel-fluid transition temperature (50 to 70 °C) and held for 2 min. Samples were then cooled at the same rate to below the gel transition temperature (-20 to −40 °C) and held for 2 min while acquiring SAXS patterns every 5 s. The entire protocol was repeated to ensure reproducibility. DSC Data was evaluated using Linksys32 V2.2.3 software, and isotopic 2D SAXS data was reduced to I(q) using the beamline software ScatterBrain.[34].

2.6. Oriented lipid bilayer samples

Oriented samples were prepared by spraying a mixture of lipids dissolved in chloroform onto a silicon substrate to approximately 2 mg cm^{-2} of lipid. After air drying, the remaining chloroform was removed by placing in a vacuum oven for 1–2 h. The samples were then left overnight in a atmosphere of 97 % RH (produced by a saturated K_2SO_4 salt solution), and then equilibrated to RH 75 % over a saturated NaCl solution. Samples for X-ray scattering were equilibrated with salt solutions containing water with natural abundance hydrogen isotopes. Samples for neutron scattering were hydrated with a saturated solution comprising 99.9 % D_2O.

2.7. Grazing incidence small angle X-ray scattering

Grazing incidence small angle X-ray scattering (GISAXS) measurements were performed on the SAXS/WAXS beamline at the Australian Synchrotron using X-rays λ = 1.033 Å (12 keV) where special care was taken to avoid sample damage with extended exposure times (∼2 s). The samples were exposed to a controlled RH environment by means of a sealed Perspex box containing a saturated NaCl solution to provide 75 % RH. The box had two mylar windows for the incident and exiting X-rays providing an uninterrupted path to the X-ray beam and detector respectively. The solid angle of the Pilatus 1 M detector was sufficient to cover 5 orders of Bragg peaks in the case of the lipid stacks considered in this work. The 2-dimenisonal scattering patterns were measured as a function of the incidence angle Ω (0.5, 0.60 and 0.65°) and converted to vertical I(q_z) and horizontal I(q_x) cuts using the NIKA macros [35] for IgorPro (Wavemetrics, Oswego, USA). The analysis focuses on those peaks whose position was not a function of Ω - i.e. the Bragg peaks.

2.8. Neutron diffraction and FTIR experiments at BioRef

Neutron diffraction measurements were made on the BioRef reflectivity beamline located in the cold neutron guide of the BER II reactor at the Lise Meitner Campus (Helmholtz Centrum Berlin, Germany).[36] The samples were placed into the beamline with a continuous stream of humid air controlled to 75 % RH. Measurements were made below and above the transition temperature of DPPC, at 30 and 55 °C. The chopper system was set to a speed of 25 Hz to cover a wave vector transfer (q_z) range from 0.003 to 0.350 $Å^{-1}$. The wavelength resolution $\Delta\lambda/\lambda$ was set to 5 %. BioRef had the capability for simultaneous *in situ* Fourier-transform infrared (FTIR) spectroscopy measurements in ATR (attenuated total reflection) geometry from the Si single crystal block using a Bruker Vertex 70 infrared spectrometer. Simultaneous measurement means that samples, and most importantly the phase transitions of the lipids, can be assessed by both methods under identical conditions in the same sample. The IR beam enters the Si substrate and is totally internally reflected several times at the sample surface before being deflected to the external IR detector. Spectra were recorded by adding 128 scans at a spectral resolution of 2 cm^{-1}. In order to provide contrast between different lipid tails the natural abundance DPPC was substituted with tail deuterated DPPC. It should be noted that there are small but well characterised differences in phase transition temperatures between the tail deuterated and natural isotopic abundance lipids, as well as small differences in their packing into bilayers.[37].

2.9. AFM experiments

The solution of SUVs were formed for surface-based investigations via self-assembly via vesicle-fusion at a freshly cleaved (refreshed) mica (muscovite) interface.[38–40] In brief, the respective solutions were pipetted onto a freshly-cleaved mica substrate, and left to equilibrate for 20 min prior to imaging. This facilitates spontaneous fusion of SUVs to the mica substrate.[38–40] This process formed either supported lipid bilayers (SLBs) or supported lipid bilayer patches (SLBPs), depending on the concentration, high or low, respectively. Each system was studied using a Cypher ES Atomic Force Microscope (Oxford Instrument, Asylum Research, Santa Barbara, CA, USA) at room temperature (25 °C) using amplitude modulated-AFM (AM-AFM). All images and force data were obtained using BioLever Mini - BL-AC40TS cantilevers (Oxford Instrument, Asylum Research, Santa Barbara, CA, USA, nominal spring constant k_c = 0.09 N/m). To minimize the imaging force, a setpoint ratio (Imaging Amplitude (A)/free amplitude (A_0)) of greater than 0.7 – 0.8 was maintained, which has been shown to minimize any tip-sample distortion and damage for a variety of materials.[41–45] Each cantilever was calibrated prior to use via the thermal spectrum method. Liquid experiments were completed in a droplet of lipid solution. This droplet was exposed to the atmosphere within an acoustic isolation cabinet (a sealed enclosure).

3. Results and discussion

3.1. Differential scanning calorimetry

DSC was used to measure the phase transitions of the individual lipids as well as their mixtures. Note that in this study RH, rather than water content, is used as the control parameter, as it allows us to compare DSC, SAXS and neutron diffraction experiments directly. Consequently, the water contents are slightly different for each sample. Most literature data is at fixed hydration, so when comparing with the literature there will be slight differences due to slight variations in the water content. It should also be noted that transition temperatures at reduced hydration are significantly higher than at full hydration (excess water). This effect is well known [46] and is not the focus of the research presented here.

Fig. 2 shows DSC thermograms of DPPC, POPC and DOPC individually and in combination at 57 % RH, which equates to ∼ 10 wt% H_2O for the three-component system (See SI). Table 1 gives the peak temperatures for each curve.

According to the literature, DPPC with ∼ 10 wt% water has a transition temperature between 50 and 60 °C [47,48] which is consistent with the value measured here (56.3 °C). Near 10 wt% H_2O, the POPC transition is reported by some to be near 10 °C,[49] while others report a very broad transition with multiple peaks between

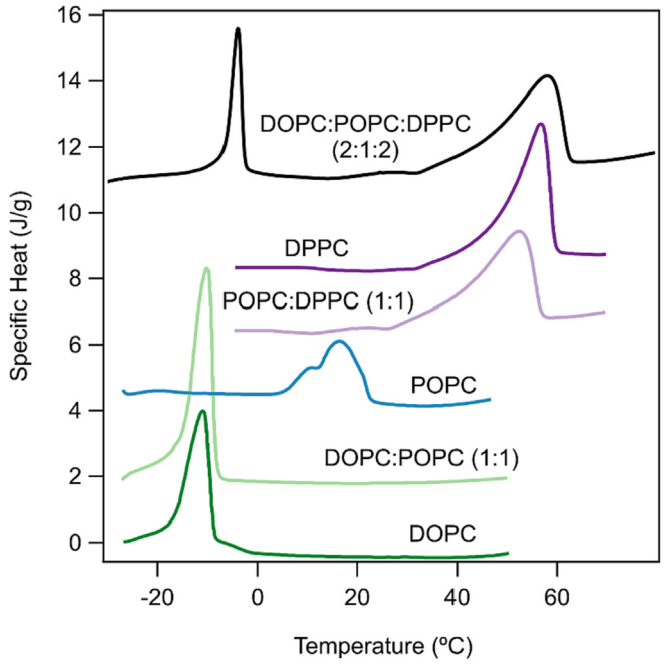

Fig. 2. DSC (heating) curves of individual, binary and ternary lipid mixtures at 57% RH. Offset in the Y-axis for clarity.

15 and 19 °C (possibly due to a very low rate of heating).[50] We found a transition at 15.4 °C for POPC at this hydration. The double peak observed in the thermogram for POPC has been previously observed,[51] and is not investigated further. In the literature, the transition temperature of DOPC at 10 wt% H_2O is approximately −15 °C,[52] slightly lower than the −11.4 °C measured here. To the authors' knowledge, no systematic studies have yet been reported on the effect of hydration on the thermal behaviour of mixtures of these lipids.

POPC's transition temperature is partway between that of DPPC and DOPC. However, when POPC is combined with either of the other lipids, its transition peak largely disappears and is instead incorporated into that of the other lipid (Fig. 2). In the case of DPPC, this causes a reduction in the combined transition temperature from 56.3 °C to 51.4 °C, as well as a broadening of the peak. This is because incorporation of POPC with its unsaturated tail means the transition to the gel phase on cooling is less energetically favourable, thus the transition is delayed to lower temperatures and broadened because of the heterogenous mixture. Microdomains of POPC transition at even lower temperatures, accounting for the small peak near 20 °C. In the literature, this mixture has only been explored in excess water where the thermogram had a broad transition stretching from −4 to 35.3 °C, with a peak near each end.[53,54] Similarly, Soloviov et al (2012) found a phase transition at around 35 °C for 1:3 mixtures of POPC:DPPC.[55] Other work using DSC on unilamellar vesicles found that the thermograms were strongly dependent on the ratio of POPC to DPPC, but even at 1:3 POPC:DPPC, the transition occurred near 35 °C in excess water.[54] Clearly the trends observed here at low hydrations are consistent with previous work in excess water, with the temperatures shifted upwards by ~ 20 °C as expected for samples at reduced hydration.[30].

The mixture of POPC and DOPC had only one peak, at −10.5 °C. Similar to the POPC:DPPC mixture, this suggests that the POPC is being incorporated into the DOPC, and its own transition is disappearing. The transition temperature of the mixture is only marginally above that of pure DOPC, suggesting only a small effect.

The three-component system consisted of DPPC, POPC and DOPC in a 2:1:2 ratio. Again, the POPC peak is almost non-existent, suggesting that the POPC is transitioning along with one or both of the other lipids. Fig. 3 shows the thermogram for the ternary system along with DOPC:DPPC 1:1 and POPC at the same RH. The data for DOPC:DPPC 1:1 demonstrates that unlike mixtures with POPC (Fig. 2), these lipids exhibit distinct transitions. The addition of POPC has a relatively small effect, broadening both transitions and shifting the DPPC transition to a lower temperature. The broadening of the high temperature peak is such that it appears to begin near the transition temperature of POPC, but there is no evidence of a separate transition for POPC. This behaviour is consistent with the observations of Hitaishi *et al.*[27].

Table 2 shows the transition temperatures for the data shown in Fig. 3. The transition temperatures of DPPC and DOPC in combination are very similar to their individual transition temperatures at these hydrations, suggesting that they have minimal influence on each other.

Fig. 4 shows the DSC heating and cooling curves of the three-component system at each RH, and the measured transition temperatures are shown in Fig. 5. All curves show similar behaviour, a low temperature peak for DOPC and a high temperature peak for DPPC. The curve for 96 % RH has shoulder peaks, strongest during heating, which are not evident at the other water contents. These shoulder peaks are most likely due to POPC transitioning, but still under the influence of DOPC or DPPC. The increased hydration at 96 % RH allows for greater lipid translational diffusion and thus better separation of these thermal events. As RH is lowered the peaks shift to higher temperatures, as expected, and broaden.

Fig. 5 shows the transition temperatures of the ternary mixture, along with the reported literature values for equivalent hydrations. The transition temperatures for the ternary mixture follow the same trends as DPPC and DOPC, shifted slightly towards intermediate temperatures, and are distinctly different from POPC (Fig. 2).

In summary, the DSC results demonstrate that the POPC preferentially transitions along with DOPC or DPPC in the mixture, rather than having a separate transition of its own, consistent with previous results.[27].

3.2. Transmission SAXS

Fig. 6 shows SAXS data for the ternary lipid mixtures at a range of temperatures for each RH. Fig. 6A shows 96 % RH, where the lipids transition from a single Lα phase at high temperatures, to a mixture of Lα and Lβ phases at intermediate temperatures before settling into a single Lβ phase at −20 °C. This is consistent with the DSC results. 57 % RH (Fig. 6C) showed the same pattern of

Table 1
DSC data for Phospholipids at 57% RH (heating).

	DPPC	DPPC:POPC 1:1	POPC	POPC:DOPC 1:1	DOPC
T Peak (°C) measured	56.3	51.4	15.4	−10.5	−11.4
T Peak (°C) literature ~10 wt% H_2O	50–60 [47,48]	–	~12 [49] 15–19 [50] 20.3 ± 0.2 [2]	–	~ −15 [52]

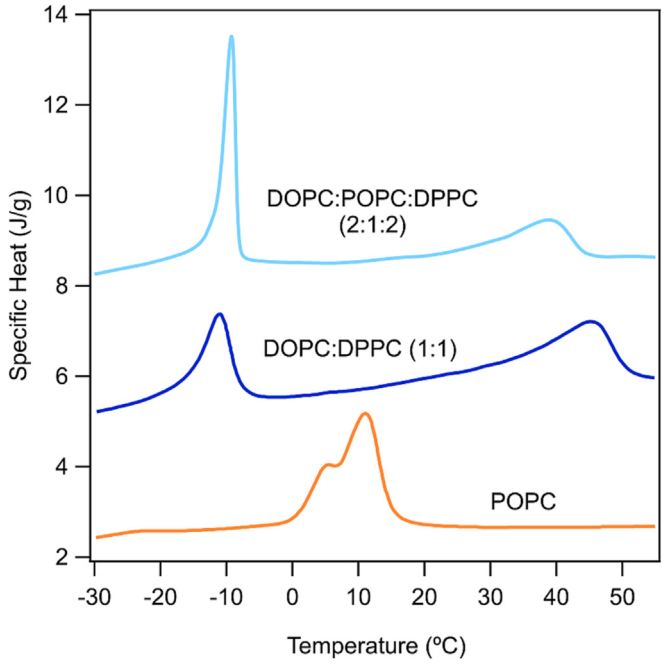

Fig. 3. DSC (heating) curves of POPC, DOPC:DPPC, and DOPC:POPC:DPPC at 75% RH.

behaviour. For the 75 % RH sample (Fig. 6B) the minimum temperature was limited to −10 °C on the lab instrument, not low enough for the sample to settle into a single L_β phase, which should occur around −15 °C based on the DSC results.

Fig. S1 shows example wide-angle scattering data with a small peak emerging at approximately q = 1.5 $Å^{-1}$ due to chain-chain reflections. The presence of this peak on cooling is due to the C16 chains transitioning from a fluid to a gel state which limits their ability to move laterally and vertically within the bilayer. Thus the packing of tail chains in the bilayer becomes more structured, and the wide-angle chain-chain peaks emerge.

Table 3 shows the measured repeat spacings calculated using linear regression based on all visible peaks for the phase at either the maximum (Lα) or minimum (Lβ) temperature scanned. As shown, there is a small increase in repeat spacing with increasing humidity (1.67 Å between 57 % and 96 % RH). There is however a significant increase of ∼ 10 Å in moving from the fluid to the gel phase. By contrast, for DPPC in excess water there is a small reduction from 67 Å (Lα at 50 °C) to 63.5 Å (Lβ at 20 °C)[56] However, the reduction in excess water is caused by two competing factors – a reduction in water thickness of 9.4 Å, accompanied by an increase in the bilayer thickness of 5.9 Å. For the dehydrated systems studied here the water thickness is constant, so any change is due to a change in bilayer thickness.

Based on these SAXS results there is no significant difference in phases formed by the ternary system compared to the individual lipids down to 57 % RH. In all cases, there is a change from an Lα phase to an Lβ phase upon cooling below the transition temperature. At relative humidities below 57 % RH, the ternary system underwent a transition to a bicontinuous cubic phase coexisting with a lamellar phase on cooling, rather than to a secondary lamellar phase (data not shown). While there is evidence of cubic phases in biological membranes,[57] they were not the focus of this investigation and so were not explored further.

3.3. Grazing incidence small angle X-ray scattering

The bulk samples measured in transmission SAXS require several days to equilibrate to a given humidity, so these equilibration times precluded a viable study of reversibility of phase behaviour on the time scale of a typical beamtime allocation. The thinner oriented lipid bilayer samples studied here, typically 1 μm thick, could be exposed to different RH values and equilibrate relatively quickly. Fig. 7 shows a typical GISAXS pattern for the Lα phase of DOPC in equilibrium with a 75 % RH atmosphere. The 2D scattering pattern shows strong peaks typical of a stack of lamellae organised parallel to the substrate. A linear regression of the *q* position for the maximum intensity for those peaks against the peak order exhibits no angular/q-dependence of the incident angle of X-rays (Ω) and yields the same repeat spacings as found in Table 3 within experimental error. The experimental errors were low compared to the peak spacing (<0.1 %) and we found that for a ∼ 20 % change in RH, the system would come to equilibrium, as measured by the repeat spacing, in typically 1–2 h. Continuous exposure of the beam on the same sample position caused visible damage and also a splitting and shift in the first order Bragg peak. To avoid these issues it was necessary to continuously translate the sample during the measurement. This strategy was easily implemented in the beamline control software.

In order to evaluate the alignment of the lamellar phase with the underlying substrate, we consider the width of the first order peaks in the q_y direction. Typically the intensity distribution is a two component line shape, a broad component which is indicative of disorder within the lamellae, and a narrower component which is indicative of the mosaic spread of the lamellae with respect to the underlying substrate.[58] For the samples studied here the registry of the bilayers on the substrate was excellent, with a mosaic spread < 0.5°. These experiments demonstrate that this approach to assembly of lipid stacks is valid, and the samples are high quality and suitable for the neutron diffraction experiments described below.

3.4. Neutron scattering and FTIR spectroscopy at BioRef

Fig. 8A shows neutron diffraction measurements from a 1:1 mixture of POPC and deuterated DPPC. The scattering curve consists of Bragg peaks superimposed on the specular reflectivity signal.[59] We assume that there is excellent registry between the plane of the Si block and the lamellae in the lipid stack. In this work we will rely only on the interpretation of Bragg peak positions rather than the reflectivity signal to extract compositional information. As was observed with SAXS, on heating, the lamellar peaks

Table 2
Peak temperature for lipids at 75% RH as shown in Fig. 3.

	DOPC:POPC:DPPC 2:1:2		DOPC:DPPC 1:1		POPC
	Low	High	Low	High	–
T_P (°C)	−10.7	35.9	−11.7	44.2	10.3
T_P (°C) Literature 15 wt% H_2O	–	–	–	–	11–17 [50]

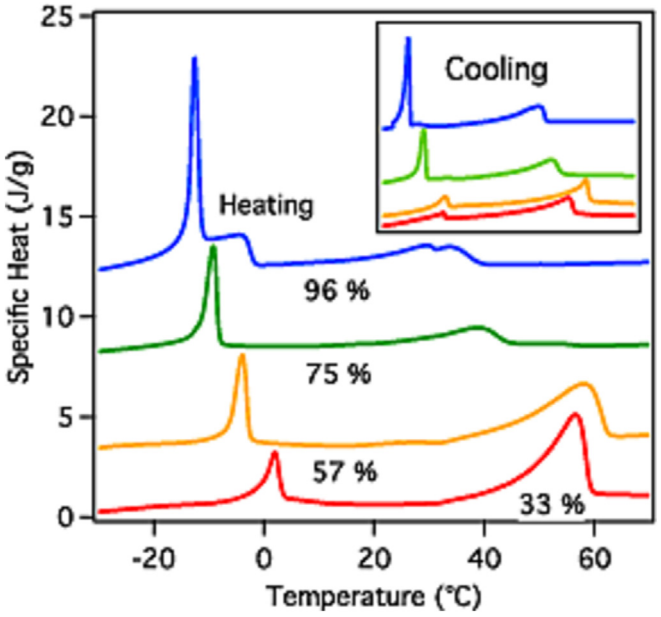

Fig. 4. DSC heating curve of DOPC:POPC:DPPC (2:1:2) ternary mixtures at the RH values indicated. Curves are vertically offset for clarity. Inset shows cooling curves over the same temperature range.

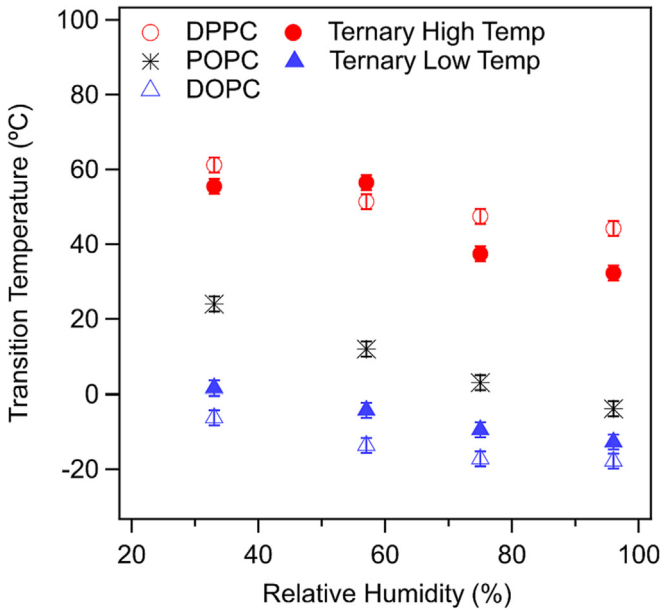

Fig. 5. Peak temperatures determined during warming for the high and low temperature transitions for the ternary DPPC:POPC:DOPC (2:1:2) mixture. For comparison, literature values are shown for the pure lipids: DPPC, [47] POPC [49] and DOPC [52].

move to higher q values and the repeat spacing reduces from 60.24 ± 1.12 to 55.99 ± 0.12 Å. As with the SAXS data, the repeat spacing was calculated using linear regression based on the visible peaks for each phase, however where only two peaks are observed, the error is based on the range, rather than the linear regression error. Previous scattering studies on the oriented DPPC system have revealed small barely resolvable differences in lamellar spacing between the tail deuterated and natural isotopic abundance lipids.[37].

The value in the fluid phase is consistent with the SAXS data for the three-component system, the observed reduction upon cooling

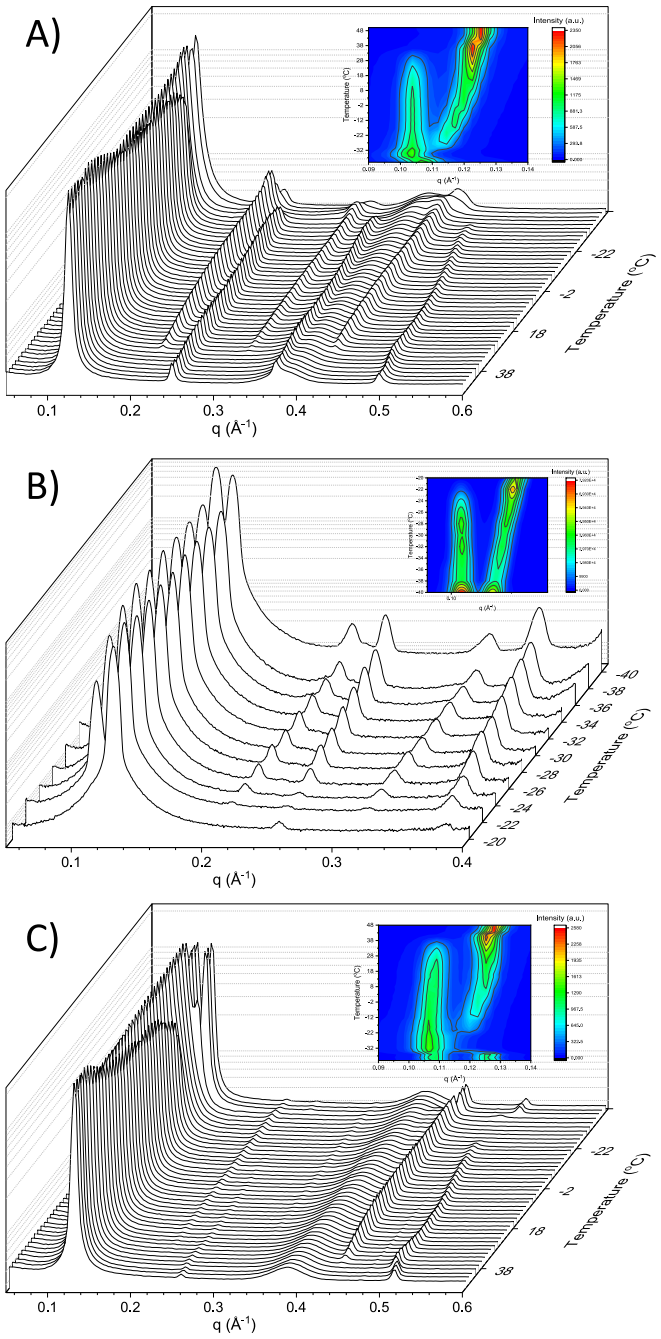

Fig. 6. A) Synchrotron SAXS patterns of DPPC:POPC:DOPC (2:1:2) at 96 % RH during cooling from 50 to −40 °C. The Lα3 peak is the sharper peak on top of the broad background peak at around q = 0.4 Å^{-1} which is due to the presence of Kapton windows; B) Lab SAXS 75 % RH H_2O during cooling from 60 to −10 °C. C) Synchrotron SAXS at 57 % RH during cooling from 70 to −20 °C. The Lα3 peak is too weak to be seen above the background. Insets show contour plots of the main peaks.

Table 3
Repeat spacings of the Lα and Lβ phase of the three-component system. Errors were determined from linear regression of the peak positions as described in Bryant et al., [29].

RH	Lα (Å)	Lβ (Å)
57 %	48.64 ± 0.02	58.78 ± 0.27
75 %	49.38 ± 0.15	59.91 ± 0.35
96 %	50.31 ± 0.16	59.99 ± 0.41

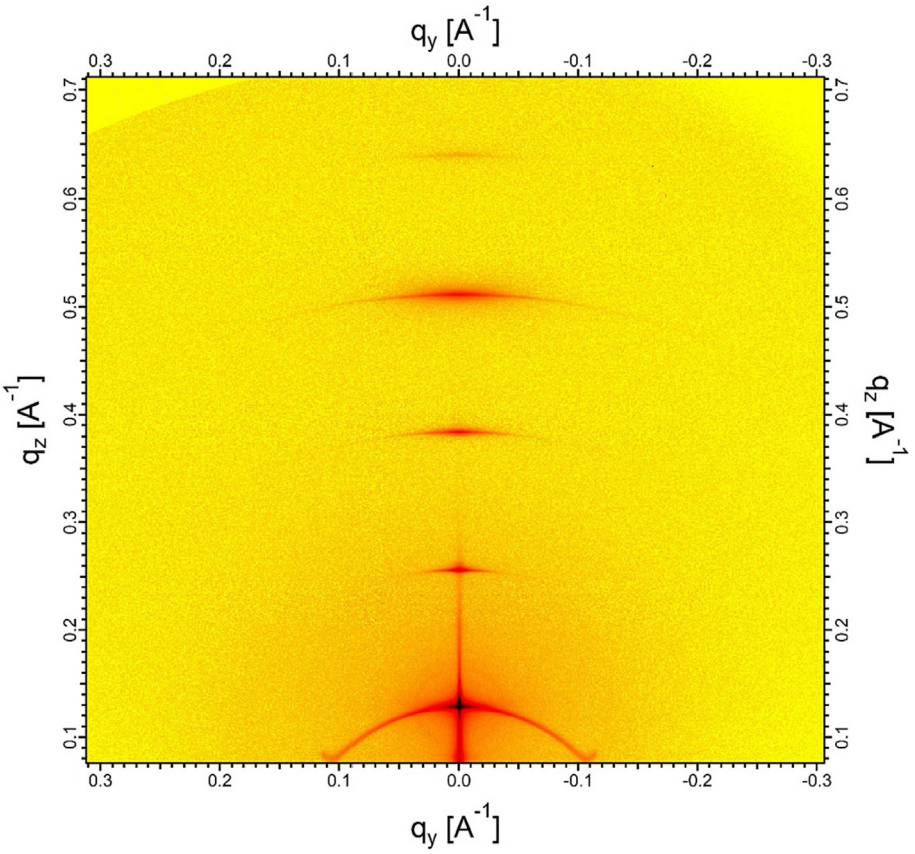

Fig. 7. Two-dimensional GISAXS image of a thin oriented lamellar stack of DOPC bilayers (25 °C, 75 % RH).

to 30 °C is smaller than would be expected for a bulk Lα to Lβ transition, however, the shift is accompanied by a strong increase in the peak labelled L_{layer}. To investigate this further IR spectra were measured simultaneously (Fig. 8) and used to monitor the structure and phase transitions of the membrane system by following the bands of the CH_2 and CD_2 vibrational modes.[60] Shown are the asymmetric and symmetric CH_2 bands at 2924 and 2853 cm^{-1}, respectively, and the corresponding bands of CD_2 with maxima at 2193 and 2088 cm^{-1}, respectively. As temperature increases, the bands move to higher wavenumbers, accompanied by a decrease in amplitude, for both the ternary mixture and the mixture of POPC with dDPPC. This is consistent with a transition from Lβ to Lα phase.[60].

In order to interpret this data, Fig. 9 illustrates some of the potential arrangements of mixed lipids in an oriented bilayer. If all lipids are mixing freely within the bilayer stack (Fig. 9 – L_{mix}) only one repeat spacing, d_{mix}, will be observed. If the different species are arranged in alternating layers (Fig. 9 – L_{layer}), there is still only one repeat spacing because the different contrasts of the two species means the neutrons can only 'see' the POPC layers. Note that this L_{layer} repeat spacing would be roughly double the normal repeat spacing and would only be observed in an oriented arrangement of stacked bilayers on a substrate – they would not be seen in SAXS samples which consist of randomly oriented multilayers. In the third scenario (Fig. 9 - L_{Sep}), there is total separation of the lipids into different micro domains, driven by the degree of saturation of the phospholipid tail, resulting in two repeat spacings, each of which are of the order of d_{mix}.

With this in mind, Fig. 8A shows a weak L_{layer} peak at 30 °C which suggests there is only a small amount of vertical phase separation of the two components - i.e. alternating layers of dDPPC in the gel phase and POPC in the fluid phase. The fact that the L_{layer} peak is weak implies that most of the lipid is still mixed, with a small fraction phase separated. As the temperature is increased to 55 °C, the whole system becomes fluid, and the L_{layer} peak becomes much stronger, suggesting a clear phase separation of the dDPPC and POPC into alternating layers (Fig. 9 – L_{layer}), enabled by the increased diffusion in the fluid phase. On returning to 30 °C the low temperature behaviour is reproduced.

Fig. 8B shows data for the 1:1 mixture of dDPPC and DOPC. At 30 °C there is a significant L_{layer} peak and only one set of main peaks (labelled $L\beta_1$). At 30 °C we know from the DSC and SAXS data that DPPC will be in the gel phase and DOPC in the fluid phase – the fact that there is a strong L_{layer} peak implies that they separate into alternating layers of fluid and gel phase (Fig. 9 – L_{layer}). However, upon heating to 55 °C where both lipids are in the fluid phase, the L_{layer} peak disappears and there are two clear sets of peaks – here the two lipids have completely phase separated into microdomains (Fig. 9 – L_{sep}). The increased temperature causes increased fluidity, and the energy cost of maintaining mixed systems with two very distinct repeat spacings becomes too high, causing the segregation of the two species, ultimately resulting in two sets of peaks. Similar behaviour has been observed previously at low hydration.[2] As with the dDPPC:POPC system, the repeat spacing reduced on heating (from 59.88 ± 0.29 to 56.12 ± 0.43 Å). The second set of peaks had a much smaller repeat spacing (43.46 ± 0.05 Å) which is significantly smaller than the reported spacings for either of these lipids [61] – however, it is known that lipids will expand laterally with increasing temperature, and so the bilayer thickness will be reduced leading to smaller repeat spacings. Once again on cooling to 30 °C the low temperature behaviour is reproduced.

Fig. 8C shows the neutron diffraction scans of the ternary mixture at 30 and 55 °C. At 30 °C there is a single set of peaks with a

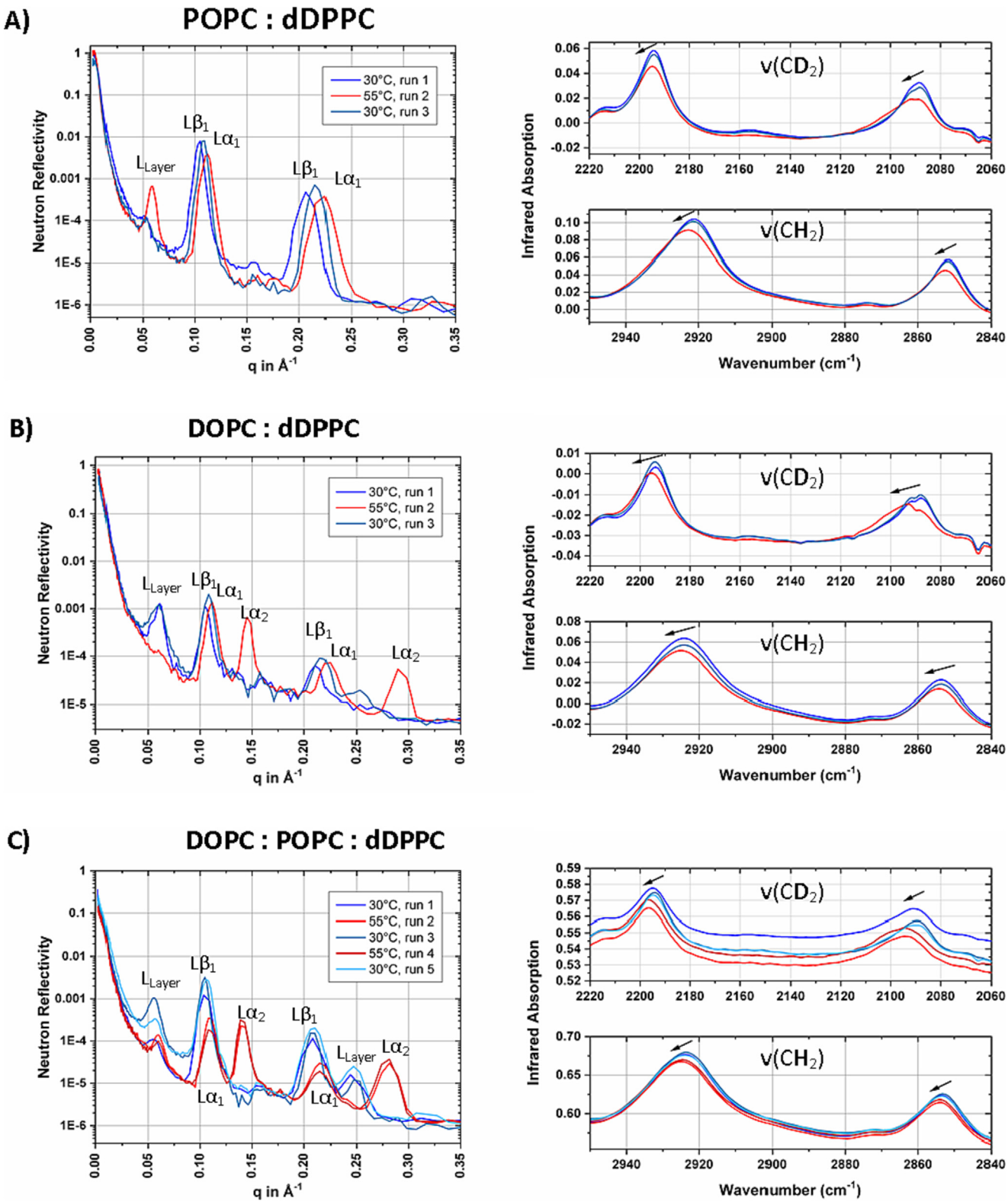

Fig. 8. Neutron diffraction (left) and FTIR spectroscopy (right) measured simultaneously at BioRef for the samples A) POPC:dDPPC (1:1) and B) DOPC:dDPPC (1:1) heated for temperature cycles from 30 °C (run 1) to 55 °C (run 2) and back to 30 °C (run 3). The mixture of C) DOPC:POPC:dDPPC (2:1:2) was measured for another heating cycle to 55 °C (run 4) and back to 30 °C (run 5). All samples were kept constantly at 75 % RH. Peak labels are referred to in the text.

repeat spacing of 60.72 ± 0.8 Å as well as a small L_{layer} peak. As the temperature is raised to 55 °C the repeat spacing shrinks to 58.40 ± 0.3 and the L_{layer} peak becomes stronger, although it is smaller than for either of the binary systems. As with the DPPC: DOPC system, a second set of peaks are visible at 55 °C. As described above, this may be a result of increased fluidity allowing segregation of the lipids. The second set of peaks again have a reduced repeat spacing of 44.80 ± 0.44 Å. The increase of the fluid-

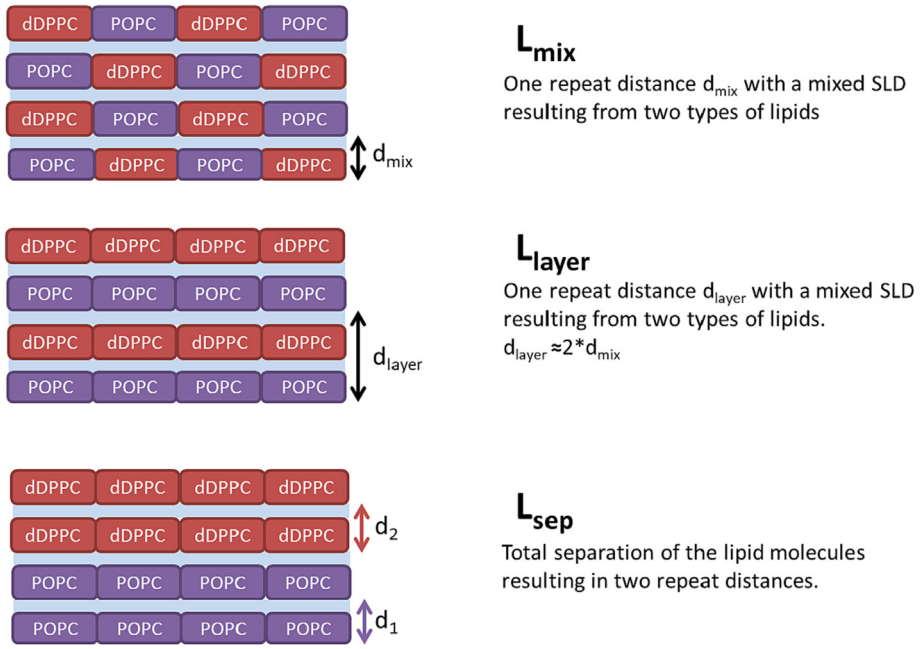

Fig. 9. Schematic illustration of possible lipid arrangements in the binary dDPPC:POPC system.

ity with higher temperature is supported by the shift to higher wavenumbers of the absorbance bands as measured simultaneously by FTIR. In order to confirm the phase transition of the ternary mixture by FTIR, the lipid mixture was also measured in a laboratory-based spectrometer, using a commercially available *in situ* unit (BioATR II, Bruker Optik GmbH, Germany). Here, the sample was heated from 20 °C to 60 °C and the shift of the absorbance bands was followed. These calibration data are in good agreement with the spectra taken at BioRef for the corresponding temperatures. The data are shown in the supplementary information (Fig. S2) for the two wavenumber regions of interest.

These results show that the presence of POPC has to have a relatively small effect, with binary and ternary mixtures showing similar behaviour.

3.5. AFM

Fig. 10 shows representative AFM images (top, middle) and force vs distance curves (bottom), colloquially referred to as "Force Curves", for the three neat lipid systems probed at low and high concentrations of 0.01 mg/mL and 0.1 mg/mL, respectively. In brief, SLBPs spontaneously form at low concentrations, whereas the underlying mica surface is completely covered by a continuous SLB at higher concentrations via the previously reported vesicle fusion method.[38–40] At low lipid concentrations, AFM images of the interface reveal raised, disc-like features of variable width. These objects are characteristic of SLBPs – regions of flat-lipid bilayer which result from SUVs rupturing, and contouring, to the underlying mica surface. Patches form at this concentration as there is not enough lipid material to achieve full surface coverage. Height analysis (see height profile, white line, bottom left of the images) reveals bilayer thicknesses of 50 Å, 61 Å, and 68 Å for DOPC, POPC, and DPPC respectively. These values are commensurate with the known thickness of the respective systems in fluid (DOPC, POPC) and gel phase (DPPC).[39,62–65] At higher concentrations (0.1 mg/mL), 5 μm × 5 μm AFM images reveal relatively homogenous surfaces, with spatially dispersed defects. For DOPC and POPC the surface structure is unremarkable, commensurate with a flat, continuous adsorbed lipid bilayer. For DPPC, the surface images appear somewhat different, with dispersed defects and spherical protrusions of ~ 400 Å in height amongst a smooth background. In this system, the large protrusions are likely a result of partially fused vesicles, which are incorporated within the underlying SLB – this is possibly due to the fact that DPPC is in the gel phase at these temperatures. Similar, partially fused lipid vesicles have been observed for SLBs in previous studies.[66].

Force data was obtained for all systems (see Fig. 10, bottom row), which provides surface normal data. In such experiments, the AFM cantilever is brought towards (approached) and away (retracted) from the interface, while the deflection of the cantilever is recorded with respect to the position of the piezoelectric stage (Z-length). For a calibrated cantilever, such as that used for these experiments, the deflection can be readily converted to a vertical force *via* Hooke's law,[67–69] and the raw Z-length mathematically converted to tip-surface separation data.[70,71] This provides apparent separation vs force data for each system, or "force curves". Once converted, this provides structural information about the bilayer systems (see Fig. 10, bottom row).

Representative force curves are provided for each system and can be interpreted as follows: At larger tip-surface separations (15–30 nm), the force curve profile remains invariant, as the motion of the cantilever is unperturbed by the presence of aqueous solution; hence, the force value here is ~ zero. Then, as the tip is brought into contact with the surface adsorbed lipid bilayers the profile begins to change, and the force rises sharply, shown as an increase in the profile. This indicates that the cantilever tip has encountered less-readily displaced material. Eventually, a "step" in the force profile is observed, where the force profile dips, becomes non-continuous, and a characteristic separation is "jumped" before the force profile again begins to rise at a tip-sample separation of ~ 0 nm. This event in the force profile of a SLB is characteristic of the cantilever tip "rupturing" the bilayer and passing through the layer until coming into contact with the surface (or as close to the surface as the cantilever tip can achieve). This distance has been colloquially termed the "rupture length" for lipid bilayers, as it is indicative of the lipid bilayer thickness. For DOPC and POPC, the rupture length was consistently observed to be ~ 5.1 nm and 6.1 nm, respectively, which is consistent with

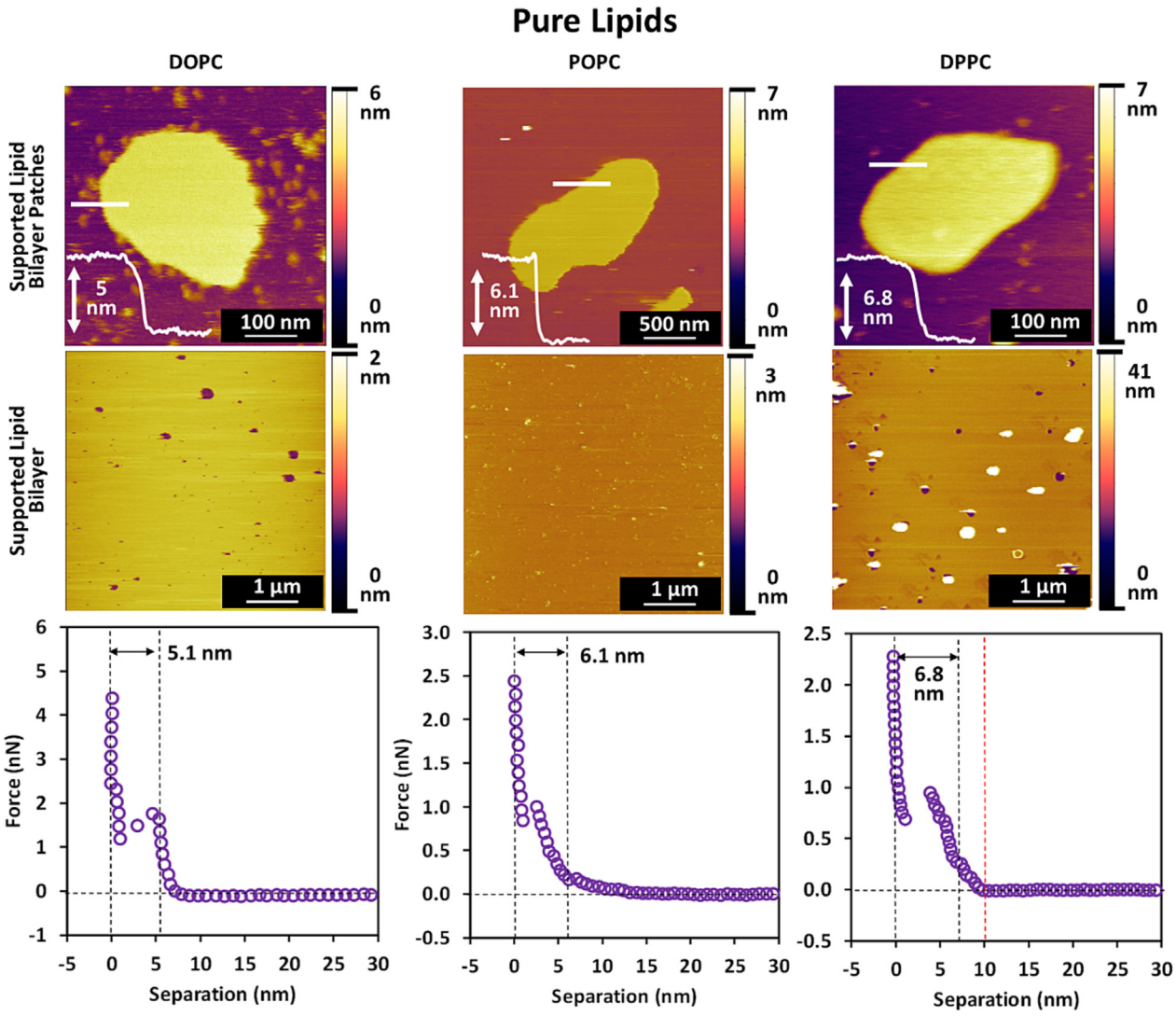

Fig. 10. Supported Lipid Bilayers at the mica interface. High-resolution AFM images of (Top) Lipid bilayer patches and (Middle) Supported lipid bilayers (SLBs) formed on a mica substrate via self-assembly (vesicle fusion method). Patches or complete bilayers are formed via variation of the lipid concentration – 0.01 mg/mL and 0.1 mg/mL lipid solutions, respectively. (Bottom) Representative force curve profiles of the SLBs. The dotted lines indicate the rupture distance as measured by the AFM cantilever during SLB compression.

their respective bilayer thicknesses and previous AFM investigations. [39,62–65] In all profiles, the onset of the bilayer rupture and zero separation has been marked with black dotted lines to better highlight this phenomenon. For DPPC, the profile appears somewhat different, with a small compressive region noted in addition to the rupture length. The onset of surface compression has been highlighted by a red dotted line for clarity. This compression likely emerges from the cantilever tip interacting with the surface-fused vesicle, which compresses under the applied load of the AFM cantilever. It should be noted that this compression was variable between force curves, indicating an inherent inhomogeneity in the sample, consistent with the AFM images of the SLB. Importantly, the measured rupture lengths of each force profile are in good agreement with the measured height of the SLBPs, meaning that both techniques are able to discern the nanoscale differences between the lipid systems.

Fig. 11 shows representative AFM images (top) and force vs distance curves (bottom) for the four mixed lipid systems investigated at a concentration of 0.1 mg/mL. For DOPC/DPPC (1:1), visual inspection of the image shows relatively flat, island-like domains surrounded by an underlying homogenous background. Section analysis from the top of one of the island-like structures to the underlying surface shows a height difference of ~ 14 Å (see white line, inset, bottom corner of image). This height difference is too small to be attributed to a single bilayer patch on the mica surface, meaning that it is likely the result of domain separation, or "lipid-rafts", occurring in the SLB. Here, the island-like structures can be attributed to an area enriched in one lipid component, while the underlying 'sea' structure is the other lipid species. Comparison between the height difference of the 'island' and the 'sea' with the measured heights of the neat systems (Fig. 10) show that the DOPC bilayer in the fluid state is ~ 17 Å thinner than that of the DPPC. As such, the height difference of 14 Å in the DOPC/DPPC (1:1) mixture indicates that we are likely observing DPPC lipid rafts, surrounded by DOPC rich regions. Force curve data for this system show a rupture length of ~ 60 Å, which is partway between that observed for either DOPC or DPPC individually, highlighting that the resulting lipid bilayer is a structural mixture of the two lipids. Bilayer defects are also observed around the intersection of the two observed phases (black spots in the image), which

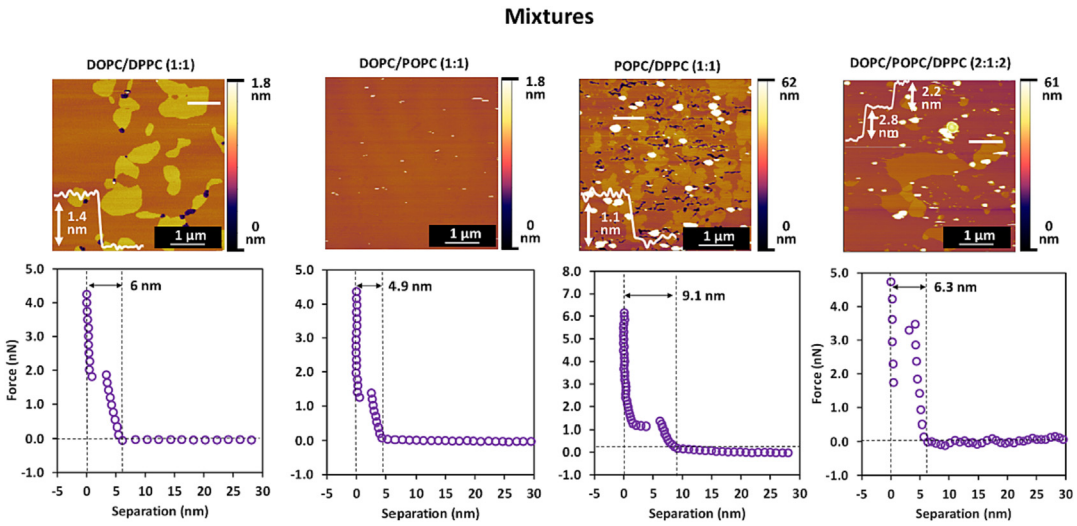

Fig. 11. Mixed Supported Lipid Bilayers at the mica interface. (Top) AFM images of the DOPC/DPPC (1:1) SLBs Lipid bilayer patches. (Bottom) Representative force curve profiles of the SLBs. The dotted lines indicate the rupture distance as measured by the AFM cantilever during SLB compression.

may result from a miss-matching in surface packing upon surface-vesicle rupture and subsequent bilayer fusion.

For DOPC/POPC (1:1), the surface structure appears homogenous without the 'islands' observed in the other mixtures. This is consistent with the two lipids being in the fluid phase and completely miscible at this temperature, unlike the behaviour observed for the DOPC:DPPC mixture. The force curve data (see Fig. 11, bottom) showed a rupture distance of 49 Å which confirms that it is a bilayer, and not the mica surface being imaged. Furthermore, this distance is similar to that observed in pure DOPC.

For POPC/DPPC (1:1), the layer appears distinctly different from the previous two systems. Here, semi-fused vesicles (large, round protrusions) are once again observed, similar to the pure DPPC system (see Fig. 10). Force profiles again show a rupture force, which indicates the presence of a well-formed bilayer, however, the rupture distance is significantly larger at ~ 91 Å than the other systems, both pure (see Fig. 10) and mixed (see Fig. 11), indicating potentially more than 1 bilayer in this system, possibly from incompletely fused vesicles. Below the vesicle protrusions, the SLB shows a distinct two-domain system, with lipid-rafts ~ 11 Å higher than the underlying lipid structure. Again, the differences observed between the sizes of the neat systems suggest that these are DPPC lipid rafts encapsulated by a "sea" of POPC-rich regions.

More interestingly, the DOPC/POPC/DPPC (2:1:2) ternary mixture shows unique, multi-tiered surface normal structures, with hints of partially fused surface vesicles. Here, islands are again seen, however, at least three distinct heights are observed in the AFM image. Section analysis shows islands that are ~ 28 Å above the 'sea' with additional artefacts that are a further 22 Å higher than the rest of the island. It is possible that these islands are composed of DPPC, surrounded by a sea of POPC and DOPC. The taller structures on top of the islands could be the remnants of semi-fused vesicles, as is observed in the POPC/DPPC and pure DPPC systems. Analysis of the force profile reveals a rupture length of ~ 63 Å, with a relatively higher force required to rupture the layer when compared to other systems which all showed similar rupture forces, which could indicate a more cohesive bilayer (consistent with DPPC being in the gel phase). As shown in Fig. 11 (4th panel) the domains sizes for the ternary system are similar to that of the DOPC:DPPC and POPC:DPPC binary systems (1st and 3rd panels) - of the order of hundreds of nm to microns, suggesting macroscopic phase separation rather than stable nanodomains. By contrast the DOPC:POPC mixture (2nd panel) appears well mixed with no large domains.

4. Discussion

The DSC results demonstrate that the POPC preferentially transitions along with DOPC or DPPC in the mixture, rather than having a separate transition of its own, consistent with previous results. [27] The SAXS results for the three-component system shows that there is a continuous transition during cooling from the fluid phase, through a coexistence region, to a gel phase at low temperatures, with no additional phases, consistent with the DSC results.

The Bragg peak positions determined by neutron diffraction on a thin layer of lipid stacks show different behaviours for the different mixtures. The dDPPC:POPC mixture appears to be reasonably well mixed at low temperatures when the dDPPC is in the gel phase, but as temperature increases there is a clear vertical phase separation of the two components (strong L_{layer} peak). By contrast the dDPPC:DOPC and ternary mixture both show clear L_{layer} peaks at 30 °C, suggesting some vertical phase separation. However, when the temperature rises to 55 °C there is macroscopic phase separation of the primary components (DOPC and dDPPC) with two clear repeat spacings. Interestingly, the presence of the POPC appears to have a relatively small effect – with very similar behaviour for the binary and ternary mixtures. This again corroborates the DSC results which found that the presence of the POPC did not qualitatively affect the phase behaviour. These results show that, at least at these reduced hydrations, POPC does not appear to be acting as a linactant – i.e. it does not reduce the extent of macroscopic phase separation taking place.

Similarly, the AFM results show that the binary and ternary mixtures all show separation of the components into large domains, with the binary and ternary mixtures similar. Again, there is no evidence of linactant behaviour, with the ternary system showing a multi-tiered structure suggesting separation of all three-components.

The results presented here contrast with previous work [1] which observed nanodomains of DPPC for similar mole ratios. The previous work found that the DPPC domain size decreased with increasing POPC mole fraction until complete mixing occurred above ~ 0.3. These differences may be due to the model

systems used - the previous work used vesicles in excess water,[1] whereas the current work used "powder" type samples and oriented membrane stacks (both at reduced hydration) and supported lipid bilayers (in excess water). It is possible that the boundary between phase separation and nanodomain formation is different depending on the model membrane system studied, and higher mole fractions of POPC may be needed to stabilise microdomains in these systems.

5. Conclusions

We have studied the phase behaviour of ternary lipid mixtures with 0.2 molar ratio of the hybrid lipid POPC using several complementary techniques. We conducted innovative neutron diffraction experiments and analysis to examine this problem in systems with reduced hydration, combined with more established techniques. We found no evidence that the hybrid lipid POPC acts as a linactant to stabilise membrane domains, regardless of hydration or temperature. Instead, there is macroscopic phase separation of the main components (DOPC and DPPC), with POPC mixing preferentially with DOPC.

This macroscopic phase separation was observed regardless of hydration or temperature and is consistent across different model membrane systems. This highlights that the most important factor in stabilising microdomains is the POPC mole fraction rather than hydration or the model membrane system employed. This raises questions about whether there are sufficiently high concentrations of such hybrid lipids in biological membranes for this to be a significant effect. It may be that the hybrid lipids do not exist in sufficient quantities to act as stabilisers and perhaps need to work in conjunction with other components (eg cholesterol). This is an important finding in relation to the role of microdomain formation and phase separation associated with membrane damage during desiccation[22] and freezing.[23,24].

This work suggests at least three avenues for further enquiry. First, a systematic study of POPC mole fraction is needed to determine if there are any conditions where microdomain formation is stabilised in such model membranes, to compare with previous studies of vesicles. Second, studies with other lipid combinations would be valuable - phosphatidylcholines have large headgroups which may dominate the interactions, so similar studies with phosphatidylethanolamines (which have much smaller headgroups) or with charged lipids may lead to different results. Third, a study of systems containing both POPC and cholesterol might reveal if there are synergistic effects in stabilising microdomains. All are needed to enable a clearer understanding of the role of hybrid lipids in stabilising microdomains across a range of biologically relevant conditions.

CRediT authorship contribution statement

Christopher J. Garvey: Conceptualization, Methodology, Investigation, Supervision, Writing – review & editing. **Saffron J. Bryant:** Investigation, Writing – review & editing. **Aaron Elbourne:** Investigation, Writing – review & editing. **Taavi Hunt:** Investigation, Writing – original draft. **Ben Kent:** Investigation, Formal analysis, Writing – review & editing. **Martin Kreuzer:** Investigation, Formal analysis, Writing – review & editing. **Markus Strobl:** Investigation, Formal analysis, Writing – review & editing. **Roland Steitz:** Investigation, Formal analysis, Writing – review & editing. **Gary Bryant:** Funding acquisition, Investigation, Supervision, Writing – review & editing.

Data availability

Data will be made available on request.

Declaration of Competing Interest

The authors declare the following financial interests/personal relationships which may be considered as potential competing interests: [Gary Bryant reports financial support was provided by Australian Research Council. Aaron Elbourne reports financial support was provided by Australian Research Council. Christopher J. Garvey reports financial support was provided by German Academic Exchange Service. Aaron Elbourne reports financial support was provided by The Jack Brockhoff Foundation. Markus Strobl reports financial support was provided by German Federal ministry for Education and Research.].

Acknowledgements

This work was facilitated by access to the SAXS/WAXS beamline at the Australian Synchrotron operated by the Australian Nuclear Science and Technology Organisation and the BIOREF neutron reflectometer at the Helmholtz Zentrum Berlin. MK acknowledges funding by the German Federal Ministry for Education and Research (BMBF) through contract no. 05KN7VH1. Dr Robert Knott is acknowledged for his support on the ANSTO laboratory Bruker SAXS instrument. The authors acknowledge the support of the ARC Research Council grants LP160101496 and DP190101010. The Cypher ES AFM instrument was funded in part by grant LE170100096 from the Australian Research Council (ARC). A.E. acknowledges support from the Jack Brockhoff Foundation (JBF Grant number 4655–2019). A.E. is supported by Australian Research Council (ARC) Discovery Early Career Research Award (DECRA) (DE220100511). This work was supported through the Australian Access to Major Research Facilities Fund (AMRF), and AINSE grants nos. 05021 and 11173. CJG acknowledges fellowships awarded from Deutsche Akademische Austauschdienst (supporting access to beamtime on the BioRef neutron reflectometer) and the Lund Institute for Advanced X-ray and Neutron Science.

Appendix A. Supplementary material

Supplementary data to this article can be found online at https://doi.org/10.1016/j.jcis.2023.01.145.

References

[1] O. Szekely, Y. Schilt, A. Steiner, U. Raviv, Regulating the size and stabilization of lipid raft-like domains and using calcium ions as their probe, Langmuir 27 (24) (2011) 14767–14775.
[2] G. Bryant, J.M. Pope, J. Wolfe, Low hydration phase properties of phospholipid mixtures, Eur. Biophys. J. 21 (3) (1992) 223–232.
[3] F. Schmid, Physical mechanisms of micro- and nanodomain formation in multicomponent lipid membranes, Biochimica et Biophysica Acta (BBA) -, Biomembranes 1859 (4) (2017) 509–528.
[4] S.J. Singer, G.L. Nicolson, The fluid mosaic model of the structure of cell membranes, Science (New York, N.Y.) 175 (1972) 720–731.
[5] K. Simons, E. Ikonen, Functional rafts in cell membranes, Nature 387 (6633) (1997) 569–572.
[6] L.J. Pike, Lipid rafts: heterogeneity on the high seas, Biochem. J. 378 (Pt 2) (2004) 281–292.
[7] L.J. Pike, Lipid rafts: bringing order to chaos, J. Lipid Res. (2003).
[8] E.L. Elson, E. Fried, J.E. Dolbow, G.M. Genin, Phase separation in biological membranes: integration of theory and experiment, Annu. Rev. Biophys. 39 (1) (2010) 207–226.
[9] B. Palmieri, T. Yamamoto, R.C. Brewster, S.A. Safran, Line active molecules promote inhomogeneous structures in membranes: theory, simulations and experiments, Adv. Colloid Interface Sci. 208 (2014) 58–65.
[10] I. Levental, S. Veatch, The continuing mystery of lipid rafts, J. Mol. Biol. 428 (24 Pt A) (2016) 4749–4764.
[11] S.L. Veatch, S.L. Keller, Seeing spots: complex phase behavior in simple membranes, Biochimica et Biophysica Acta, Molecular Cell Research 1746 (3) (2005) 172–185.
[12] R. Brewster, P.A. Pincus, S.A. Safran, Hybrid lipids as a biological surface-active component, Biophys J 97 (4) (2009) 1087–1094.

[13] R. Brewster, S.A. Safran, Line active hybrid lipids determine domain size in phase separation of saturated and unsaturated lipids, Biophys. J. 98 (6) (2010) L21–L23.
[14] T. Yamamoto, R. Brewster, S.A. Safran, Chain ordering of hybrid lipids can stabilize domains in saturated/hybrid/cholesterol lipid membranes, EPL (Europhys. Lett.) 91 (2) (2010) 28002.
[15] H.J. Risselada, S.J. Marrink, The molecular face of lipid rafts in model membranes, Proc. Natl. Acad. Sci. 105 (45) (2008) 17367–17372.
[16] D.G. Ackerman, G.W. Feigenson, Multiscale modeling of four-component lipid mixtures: domain composition, size, alignment, and properties of the phase interface, J. Phys. Chem. B 119 (11) (2015) 4240–4250.
[17] F.A. Heberle, M. Doktorova, S.L. Goh, R.F. Standaert, J. Katsaras, G.W. Feigenson, Hybrid and nonhybrid lipids exert common effects on membrane raft size and morphology, J. Am. Chem. Soc. 135 (40) (2013) 14932–14935.
[18] P.F. Almeida, How to determine lipid interactions in membranes from experiment through the ising model, Langmuir 35 (1) (2019) 21–40.
[19] R.D. Usery, T.A. Enoki, S.P. Wickramasinghe, M.D. Weiner, W.-C. Tsai, M.B. Kim, S. Wang, T.L. Torng, D.G. Ackerman, F.A. Heberle, J. Katsaras, G.W. Feigenson, Line tension controls liquid-disordered + liquid-ordered domain size transition in lipid bilayers, Biophys J 112 (7) (2017) 1431–1443.
[20] A.A. Bischof, A. Mangiarotti, N. Wilke, Searching for line active molecules on biphasic lipid monolayers, Soft Matter 11 (11) (2015) 2147–2156.
[21] F.A. Heberle, R.S. Petruzielo, J. Pan, P. Drazba, N. Kučerka, R.F. Standaert, G.W. Feigenson, J. Katsaras, Bilayer thickness mismatch controls domain size in model membranes, J. Am. Chem. Soc. 135 (18) (2013) 6853–6859.
[22] F.A. Hoekstra, E.A. Golovina, J. Buitink, Mechanisms of plant desiccation tolerance, Trends Plant Sci. 6 (9) (2001) 431–438.
[23] J. Wolfe, G. Bryant, Cellular cryobiology: thermodynamic and mechanical effects, Int. J. Refrigeration-Revue Internationale du Froid 24 (5) (2001) 438–450.
[24] P.J. Quinn, A lipid-phase separation model of low-temperature damage to biological membranes, Cryobiology 22 (2) (1985) 128–146.
[25] S.-M. Liang, J.-F. Kuang, S.-J. Ji, Q.-F. Chen, W. Deng, T. Min, W. Shan, J.-Y. Chen, W.-J. Lu, The membrane lipid metabolism in horticultural products suffering chilling injury, Food Qual. Saf. 4 (1) (2020) 9–14.
[26] T. Crul, B. Csoboz, I. Gombos, A. Marton, M. Peter, G. Balogh, C. Vizler, L. Szente, L. Vigh, Modulation of plasma membrane composition and microdomain organization impairs heat shock protein expression in B16–F10 mouse melanoma cells, Cells 9 (4) (2020).
[27] P. Hitaishi, P. Mandal, S.K. Ghosh, Partitioning of a hybrid lipid in domains of saturated and unsaturated lipids in a model cellular membrane, ACS Omega 6 (50) (2021) 34546–34554.
[28] G. Bryant, J. Wolfe, Can hydration forces induce lateral phase separations in lamellar phases?, Eur Biophys. J. 16 (6) (1989) 369–374.
[29] G. Bryant, M.B. Taylor, T.A. Darwish, A.M. Krause-Heuer, B. Kent, C.J. Garvey, Effect of deuteration on the phase behaviour and structure of lamellar phases of phosphatidylcholines - Deuterated lipids as proxies for the physical properties of native bilayers, Colloids Surf. B-Biointerfaces 177 (2019) 196–203.
[30] G. Bryant, J. Wolfe, Interfacial Forces in Cryobiology and Anhydrobiology, Cryo-Letters 13 (1) (1992) 23–36.
[31] L.B. Rockland, Saturated salt solutions for static control of relative humidity between 5-degrees-C and 40-degrees-C, Anal. Chem. 32 (10) (1960) 1375–1376.
[32] W. Trewby, D. Livesey, K. Voitchovsky, Buffering agents modify the hydration landscape at charged interfaces, Soft Matter 12 (9) (2016) 2642–2651.
[33] N.M. Kirby, S.T. Mudie, A.M. Hawley, D.J. Cookson, H.D.T. Mertens, N. Cowieson, V. Samardzic-Boban, A low-background-intensity focusing small-angle X-ray scattering undulator beamline, J. Appl. Cryst. 46 (2013) 1670–1680.
[34] S.T. Mudie, D. Cookson, N. Kirby, A. Hawley, H.D.T. Mertens, scatterBrain: An Advanced Software Package for Small Angle Scattering Data Acquisition, Reduction, and Analysis, in: D.J. McGillivray, J. Trewhella, E.P. Gilbert, T.L. Hanley (Eds.) 15th International Small-Angle Scattering Conference, Australian Nuclear Science and Technology Organisation, Sydney, 2012.
[35] J. Ilavsky, Nika: software for two-dimensional data reduction, J. Appl. Cryst. 45 (2) (2012) 324–328.
[36] M. Strobl, R. Steitz, M. Kreuzer, M. Rose, H. Herrlich, F. Mezei, M. Grunze, R. Dahint, BioRef: a versatile time-of-flight reflectometer for soft matter applications at Helmholtz-Zentrum Berlin, Rev. Sci. Instrum. 82 (5) (2011) 055101.
[37] G. Bryant, M.B. Taylor, T.A. Darwish, A.M. Krause-Heuer, B. Kent, C.J. Garvey, Effect of deuteration on the phase behaviour and structure of lamellar phases of phosphatidylcholines – deuterated lipids as proxies for the physical properties of native bilayers, Colloids Surf. B: Biointerfaces (2019).
[38] H.M. Seeger, A.D. Cerbo, A. Alessandrini, P. Facci, Supported lipid bilayers on mica and silicon oxide: comparison of the main phase transition behavior, J. Phys. Chem. B 114 (27) (2010) 8926–8933.
[39] Z. Lv, S. Banerjee, K. Zagorski, Y.L. Lyubchenko, Supported lipid bilayers for atomic force microscopy studies, MethodsMol. Biol. 2018 (1814) 129–143.
[40] B. Seantier, C. Breffa, O. Félix, G. Decher, In situ investigations of the formation of mixed supported lipid bilayers close to the phase transition temperature, Nano Lett. 4 (1) (2004) 5–10.
[41] R. García, Amplitude Modulation AFM in Liquid, Amplitude Modulation Atomic Force Microscopy, Wiley-VCH Verlag GmbH & Co. KGaA2010, pp. 77-90.
[42] K. Voitchovsky, Anharmonicity, solvation forces, and resolution in atomic force microscopy at the solid-liquid interface, Phys. Rev. E 88 (2) (2013).
[43] A.J. Page, A. Elbourne, R. Stefanovic, M.A. Addicoat, G.G. Warr, K. Voitchovsky, R. Atkin, 3-Dimensional atomic scale structure of the ionic liquid-graphite interface elucidated by AM-AFM and quantum chemical simulations, Nanoscale 6 (14) (2014) 8100–8106.
[44] A. Elbourne, S. McDonald, K. Voïchovsky, F. Endres, G.G. Warr, R. Atkin, Nanostructure of the ionic liquid-graphite stern layer, ACS Nano 9 (7) (2015) 7608–7620.
[45] A. Elbourne, B. McLean, K. Voïtchovsky, G.G. Warr, R. Atkin, Molecular resolution in situ imaging of spontaneous graphene exfoliation, J. Phys. Chem. Lett. 7 (16) (2016) 3118–3122.
[46] G. Cevc, D. Marsh, Hydration of noncharged lipid bilayer membranes. Theory and experiments with phosphatidylethanolamines, Biophys. J. 47 (1) (1985) 21–31.
[47] M. Kodama, M. Kuwabara, S. Seki, Successive phase-transition phenomena and phase diagram of the phosphatidylcholine-water system as revealed by differential scanning calorimetry, Biochimica et Biophysica Acta (BBA) - Biomembranes 689 (3) (1982) 567–570.
[48] C. D'Ambrosio, L. Powers, Optical studies of the phase behavior of monodomain samples of dipalmitoyl phosphatidylcholine containing calcium chloride, Biophys. J. 27 (1) (1979) 15–20.
[49] D.V. Lynch, P.L. Steponkus, Lyotropic phase behavior of unsaturated phosphatidylcholine species: relevance to the mechanism of plasma membrane destabilization and freezing injury, Biochimica et Biophysica Acta (BBA) - Biomembranes 984 (3) (1989) 267–272.
[50] H. Pfeiffer, G. Klose, K. Heremans, Reorientation of hydration water during the thermotropic main phase transition of 1-palmitoyl-2-oleolyl-sn-glycero-3-phosphocholine (POPC) bilayers at low degrees of hydration, Chem. Phys. Lett. 572 (2013) 120–124.
[51] K.L. Koster, K.J. Maddocks, G. Bryant, Exclusion of maltodextrins from phosphatidylcholine multilayers during dehydration: effects on membrane phase behaviour, Eur. Biophys. J. 32 (2) (2003) 96–105.
[52] M.S. Webb, H. Sek Wen, P.L. Steponkus, Dehydration-induced lamellar-to-hexagonal-II phase transitions in DOPE/DOPC mixtures, Biochimica et Biophysica Acta (BBA) -, Biomembranes 1145 (1) (1993) 93–104.
[53] W. Curatolo, B. Sears, L.J. Neuringer, A calorimetry and deuterium NMR study of mixed model membranes of 1-palmitoyl-2-oleylphosphatidylcholine and saturated phosphatidylcholines, Biochimica et Biophysica Acta (BBA) -, Biomembranes 817 (2) (1985) 261–270.
[54] J.A. Svetlovics, S.A. Wheaten, P.F. Almeida, Phase separation and fluctuations in mixtures of a saturated and an unsaturated phospholipid, Biophys J 102 (11) (2012) 2526–2535.
[55] D.V. Soloviov, Y.E. Gorshkova, O.I. Ivankov, A.N. Zhigunov, L.A. Bulavin, V.I. Gordeliy, A.I. Kuklin, Ripple phase behaviour in mixtures of DPPC/POPC Lipids: SAXS and SANS studies, J. Phys. Conf. Ser. 351 (2012).
[56] J.F. Nagle, S. Tristram-Nagle, Structure of lipid bilayers, Biochimica et Biophysica Acta (BBA) – Rev. Biomembranes 1469 (3) (2000) 159–195.
[57] Z.A. Almsherqi, S.D. Kohlwein, Y. Deng, Cubic membranes: a legend beyond the Flatland* of cell membrane organization, J. Cell Biol. 173 (6) (2006) 839–844.
[58] P. Stepanek, F. Nallet, O. Diat, K. Almdal, P. Panine, Undulation properties of the lamellar phase of a diblock copolymer: SAXS experiments, Macromolecules 35 (19) (2002) 7287–7292.
[59] U. Mennicke, T. Salditt, Preparation of solid-supported lipid bilayers by spin-coating, Langmuir 18 (21) (2002) 8172–8177.
[60] R. Lewis, R.N. McElhaney, Membrane lipid phase transitions and phase organization studied by Fourier transform infrared spectroscopy, Biochimica Et Biophysica Acta-Biomembranes 1828 (10) (2013) 2347–2358.
[61] G. Bryant, M.B. Taylor, T.A. Darwish, A.M. Krause-Heuer, B. Kent, C.J. Garvey, Effect of deuteration on the phase behaviour and structure of lamellar phases of phosphatidylcholines – Deuterated lipids as proxies for the physical properties of native bilayers, Colloids Surf. BBiointerfaces 177 (2019) 196–203.
[62] E.I. Goksu, J.M. Vanegas, C.D. Blanchette, W.-C. Lin, M.L. Longo, AFM for structure and dynamics of biomembranes, Biochimica et Biophysica Acta (BBA) - Biomembranes 1788 (1) (2009) 254–266.
[63] S.F. Gilmore, D.Y. Sasaki, A.N. Parikh, Thermal annealing triggers collapse of biphasic supported lipid bilayers into multilayer islands, Langmuir 30 (17) (2014) 4962–4969.
[64] S.J. Attwood, Y. Choi, Z. Leonenko, Preparation of DOPC and DPPC supported planar lipid bilayers for atomic force microscopy and atomic force spectroscopy, Int. J. Mol. Sci. 14 (2) (2013) 3514–3539.
[65] M.J. Higgins, M. Polcik, T. Fukuma, J.E. Sader, Y. Nakayama, S.P. Jarvis, Structured water layers adjacent to biological membranes, Biophys J 91 (7) (2006) 2532–2542.
[66] I. Reviakine, A. Brisson, Formation of supported phospholipid bilayers from unilamellar vesicles investigated by atomic force microscopy, Langmuir 16 (4) (2000) 1806–1815.
[67] J.E. Sader, I. Larson, P. Mulvaney, L.R. White, Method for the calibration of atomic force microscope cantilevers, Rev. Sci. Instrum. 66 (7) (1995) 3789–3798.
[68] J.E. Sader, J.W. Chon, P. Mulvaney, Calibration of rectangular atomic force microscope cantilevers, Rev. Sci. Instrum. 70 (10) (1999) 3967–3969.
[69] B. Cappella, G. Dietler, Force-distance curves by atomic force microscopy, Surf. Sci. Rep. 34(1-3) (1999) 1-+.
[70] R. Garcia, R. Perez, Dynamic atomic force microscopy methods, Surf. Sci. Rep. 47 (6–8) (2002) 197–301.
[71] T.J. Senden, Force microscopy and surface interactions, Curr. Opin. Colloid Interface Sci. 6 (2) (2001) 95–101.